Chemistry and Physics of Lipids 178 (2014) 1–10

Contents lists available at ScienceDirect

Chemistry and Physics of Lipids

journal homepage: www.elsevier.com/locate/chemphyslip

X-ray structure, thermodynamics, elastic properties and MD simulations of cardiolipin/dimyristoylphosphatidylcholine mixed membranes

Alexander L. Boscia[a], Bradley W. Treece[a], Dariush Mohammadyani[b], Judith Klein-Seetharaman[c], Anthony R. Braun[d], Tsjerk A. Wassenaar[e], Beate Klösgen[f], Stephanie Tristram-Nagle[a,*]

[a] Biological Physics Group, Physics Department, Carnegie Mellon University, Pittsburgh, PA 15213, United States
[b] Bioengineering Department, University of Pittsburgh, Pittsburgh, PA 15260, United States
[c] Metabolic & Vascular Health, Medical School, University of Warwick, Coventry, England CV4 7AL, United Kingdom
[d] Department of Biomedical Engineering, University of Minnesota, Minneapolis, MN 55455, United States
[e] Groningen Biomolecular Sciences and Biotechnology Institute and Zernike Institute for Advanced Materials, University of Groningen, Nijenborgh 7, 9747 AG Groningen, The Netherlands
[f] Department of Physics, Chemistry and Pharmacy, University of Southern Denmark, DK-5230 Odense M, Denmark

ARTICLE INFO

Article history:
Received 5 November 2013
Received in revised form
18 December 2013
Accepted 20 December 2013
Available online 28 December 2013

Keywords:
Lipid bilayer structure
Differential scanning calorimetry
X-ray diffuse scattering
LAXS
WAXS
DMPC

ABSTRACT

Cardiolipins (CLs) are important biologically for their unique role in biomembranes that couple phosphorylation and electron transport like bacterial plasma membranes, chromatophores, chloroplasts and mitochondria. CLs are often tightly coupled to proteins involved in oxidative phosphorylation. The first step in understanding the interaction of CL with proteins is to obtain the pure CL structure, and the structure of mixtures of CL with other lipids. In this work we use a variety of techniques to characterize the fluid phase structure, material properties and thermodynamics of mixtures of dimyristoylphosphatidylcholine (DMPC) with tetramyristoylcardiolipin (TMCL), both with 14-carbon chains, at several mole percentages. X-ray diffuse scattering was used to determine structure, including bilayer thickness and area/lipid, the bending modulus, K_C, and S_{Xray}, a measure of chain orientational order. Our results reveal that TMCL thickens DMPC bilayers at all mole percentages, with a total increase of ~6 Å in pure TMCL, and increases A_L from 64 Å^2 (DMPC at 35 °C) to 109 Å^2 (TMCL at 50 °C). K_C increases by ~50%, indicating that TMCL stiffens DMPC membranes. TMCL also orders DMPC chains by a factor of ~2 for pure TMCL. Coarse grain molecular dynamics simulations confirm the experimental thickening of 2 Å for 20 mol% TMCL and locate the TMCL headgroups near the glycerol-carbonyl region of DMPC; i.e., they are sequestered below the DMPC phosphocholine headgroup. Our results suggest that TMCL plays a role similar to cholesterol in that it thickens and stiffens DMPC membranes, orders chains, and is positioned under the umbrella of the PC headgroup. CL may be necessary for hydrophobic matching to inner mitochondrial membrane proteins. Differential scanning calorimetry, S_{Xray} and CGMD simulations all suggest that TMCL does not form domains within the DMPC bilayers. We also determined the gel phase structure of TMCL, which surprisingly displays diffuse X-ray scattering, like a fluid phase lipid. A_L = 40.8 Å^2 for the ½TMCL gel phase, smaller than the DMPC gel phase with A_L = 47.2 Å^2, but similar to A_L of DLPE = 41 Å^2, consistent with untilted chains in gel phase TMCL.

Abbreviations: CL, cardiolipin; TMCL, tetramyristoylcardiolipin; TMCL, ½TMCL; DMPC, dimyristoylphosphocholine; PC, phosphocholine; DPPC, dipalmitoylphosphocholine; DPPE, dipalmitoylphosphoethanolamine; DMPE, dimyristoylphosphocholine; DLPE, dilauroylphosphocholine; LAXS, low-angle X-ray scattering; WAXS, wide-angle X-ray scattering; CGMD, coarse grain molecular dynamics; TFE, trifluoroethanol; MLVs, multilamellar vesicles; CHESS, Cornell High Energy Synchrotron Source; DSC, differential scanning calorimetry; NVT, canonical ensemble (*N*, number of moles, *V*, volume, *T*, temperature, all conserved); NPT, isobaric–isothermal ensemble; IMMs, inner mitochondrial membranes.

* Corresponding author. Tel.: +1 412 268 3174; fax: +1 412 681 0648; mobile: +1 412 680 8640.
E-mail address: stn@cmu.edu (S. Tristram-Nagle).

0009-3084/$ – see front matter © 2013 Elsevier Ireland Ltd. All rights reserved.
http://dx.doi.org/10.1016/j.chemphyslip.2013.12.010

1. Introduction

Cardiolipin (CL) refers to a group of unusual glycerophospholipids which contain four instead of two acyl chains. The acyl chain composition varies with species and cell state. CL's headgroup is negatively charged at pH 7.0 due to two phosphate groups with pK_a's ~3 and >8 (Kates et al., 1993) connected by a glycerol moiety. Many investigations have been carried out to characterize CL's overall structure (Lewis et al., 2007), headgroup structure (Haines, 2009; Tarahovsky et al., 2000), thermodynamic properties (Lewis and McElhaney, 2009; Nichols-Smith et al., 2004), water permeability (Shibata et al., 1994), membrane fluidity (Yamauchi et al., 1981), ability to form the hexagonal II (H_{II}) phase (Powell and Hui, 1996; Powell and Marsh, 1985; Rand and Sengupta, 1972; Seddon et al., 1983) and domains when mixed with other host phospholipids (Domenech et al., 2007; Frias et al., 2011; Lupi et al., 2008; Pinheiro et al., 1994; Sennato et al., 2005). Molecular dynamics simulations have been carried out to determine the structure of CL in bilayers (Dahlberg, 2007; Dahlberg and Maliniak, 2008) and the hydrogen-bonding capability of its headgroup (Dahlberg et al., 2010). However, comparisons between different studies and techniques are difficult due to different chain compositions. In this work we present results from experiments and simulations; in both cases, CL contains the same chains as the host lipid, DMPC (dimyristoylphosphatidylcholine).

The keen interest in CL emanates from its important biological roles. CLs are unique to biomembranes that couple phosphorylation and electron transport: bacterial plasma membranes, chromatophores, chloroplasts and mitochondria (Hoch, 1992). CL is necessary for proper ADP/ATP carrier function and/or formation of protein supercomplexes (Claypool et al., 2008; Hoffmann et al., 1994; Pfeiffer et al., 2003; Zhang et al., 2002). CL has been shown to co-isolate with each of the proteins that participate in oxidative phosphorylation: cytochrome oxidase (Robinson, 1993), ATP/ADP exchange protein (Horvath et al., 1990), F_0F_1 ATP synthase (Eble et al., 1990), the orthophosphate transporter (Kaplan et al., 1986) and the cytochrome bc_1 complex (Yu et al., 1978). It has been suggested that CL's role is to serve as a proton trap for oxidative phosphorylation due to the acid-anion nature of its unique headgroup (Haines and Dencher, 2002). Alternative roles for CL include the formation of cubic phases which can efficiently store lipid for the dynamic cristae (Deng and Mieczkowski, 1998) and apoptosis signaling (Kagan et al., 2009). Especially, CL seems to play a crucial role in the assembly of a passive docking platform for the binding of Bid, and the initiation of the apoptotic process (Jalmar et al., 2013). Finally, a defect in CL synthesis is the cause of Barth's syndrome, which is a sex-linked recessive disorder, clinically characterized by the classical symptoms of cardiomyopathy, neutropenia and delayed growth with a lethal effect on young boys (Barth et al., 1983). It is thought that a defective CL cannot interact with the proteins involved in energy production in the mitochondria. In rat liver mitochondria, CL contains chains with primarily C18:2 fatty acids (Daum, 1985), symmetrically (Schlame et al., 2005). In Barth's syndrome, chain symmetry is lost, which could account for CL's inability to interact with proteins (Schlame et al., 2005).

CL is synthesized exclusively on the inner mitochondrial membrane (IMM) (Hostetler and Van den Bosch, 1972; Jelsema and Morre, 1978) and except for a small amount of phosphatidylinositol, CL is the only negatively charged lipid in mitochondria (Hovius et al., 1990). There is ~20% (by weight) CL in eukaryotic mitochondria, where ~3/4 resides in the IMM (Daum, 1985). The major portion (75–90%) of CL in the IMM is located on the matrix side (Daum, 1985). CL is 9.2 mol% of total IMM lipids (Gomez and Robinson, 1999). Since most CL is located on the matrix side, the local concentration of CL could be as high as ~20 mol% CL, but because CL can be found associated with proteins and is also transferred across the membrane, its concentration will vary based on location and state of the cell. In this work we therefore explored many mole ratios of tetramyristoylCL (TMCL) including pure TMCL for comparison, but focused on 20 mol% for the coarse-grained MD simulations as a matrix side mimic of IMM. We mixed TMCL with dimyristoylphosphatidylcholine (DMPC), where TMCL contains the same chains as DMPC, C14:0. Although the chains of CL in eukaryotic mitochondria are primarily unsaturated, investigation of mixtures with identical chains rules out chain immiscibility as a cause of phase separation. We use low-angle X-ray diffuse scattering (LAXS) to obtain the structure (bilayer thickness and area) and bending modulus (K_C), and wide-angle X-ray scattering (WAXS) to obtain the S_{Xray} order parameter of TMCL/DMPC mixtures in the fluid phase. Densimetry determines the molecular volumes which are needed for electron density profiles, while differential scanning calorimetry determines the T_m's (main transition melting temperatures). LAXS is also used to determine the structure of pure TMCL in the gel phase. The experimental work was complemented with coarse-grain Martini molecular dynamics simulations to obtain a comprehensive view on the underlying processes.

2. Materials and methods

2.1. Samples

Purified lipids were purchased from Avanti Polar Lipids (Alabaster, AL) and used without further purification. DMPC Lots #140PC-226 and #140PC-256, and TMCL Lots #140CA-40 and #140CA-51 as the NH_4^+ salt were used. Thin layer chromatography (TLC) revealed that Lot #140CA-40 TMCL contained <1% lysolecithin and that Lot #140CA-51 TMCL contained <0.1% lysolecithin before the experiments. Lipid stocks solutions were prepared by precisely weighing lyophilized lipid into glass vials and HPLC chloroform was added; these stock solutions were aliquoted into glass test tubes to generate the mole percentages: 0, 0.7, 2.7, 4.4, 10, 20 and 100 TMCL/(DMPC + TMCL). When these concentrations are converted into chain concentrations, 2TMCL/(DMPC + 2TMCL), where TMCL = ½TMCL, they become 0, 1.39, 5.26, 8.43, 33.33 and 100. For X-ray scattering, 4 mg lipid mixture in 200 μl HPLC chloroform:trifluoroethanol (TFE) (1:1, v:v) was plated onto silicon wafers (15 mm × 30 mm × 1 mm) via the rock and roll method (Tristram-Nagle, 2007) to produce ~1800 well-aligned bilayers. Solvents were thoroughly removed, first by evaporation for one day in the fume hood, then by evaporation under vacuum for at least two hours. Samples were hydrated through the vapor in a thick-walled X-ray hydration chamber (Kučerka et al., 2005a) for 0.5–1 h. For X-ray capillary experiments, multilamellar vesicles (MLVs) were prepared by mixing dried lipid mixtures with MilliQ water or 50 mM Hepes buffer, pH 7.0, to a final concentration of 25 wt% and cycling three times between −20 °C and 50 °C for ten minutes at each temperature with vortexing; this suspension was loaded into X-ray capillaries (Charles Supper, Cambridge, MA). For densimetry, MLVs at 5 wt% in water were hydrated as above. For calorimetry, MLVs at a concentration of 0.1% in water were hydrated as for densimetry.

2.2. Volume determination

Volumes of fully hydrated MLVs of DMPC/TMCL lipid mixtures and pure lipids were determined as a function of temperature from 20 ± 0.01 °C to 55 ± 0.01 °C using an Anton-Paar USA DMA5000M (Ashland, VA) vibrating tube densimeter (Raghunathan et al., 2012). After densimetry, TLC revealed ~2% lysolecithin.

2.3. X-ray scattering and liquid crystal analysis

2.3.1. LAXS

Low-angle X-ray scattering (LAXS) data from oriented fluid phase lipid mixtures at 35, 40 and 50 °C were obtained on three separate trips to the Cornell High Energy Synchrotron Source (CHESS) using previously described methods (Kučerka et al., 2005a; Liu and Nagle, 2004; Lyatskaya et al., 2001). Typical beam width was 0.25 mm and beam height was 1–1.2 mm. Typical wavelength was 1.18 Å with a total beam intensity of $\sim(1–5)\times10^{11}$ photons/(s mm^2). Typical sample-to-CCD distance was 365 mm (LAXS) and 156 mm (WAXS), calibrated using a silver behenate standard with *D*-spacing 58.4 Å. Temperature was controlled with a Julabo F25 (Allentown, PA). After X-ray at CHESS, we measured ~5% breakdown in samples held at the lower temperatures, and 20% breakdown in samples held at 50 °C.

2.3.2. Structural analysis

The X-ray $|F(q_z)|$ data were fit to the Fourier transform of a model of the electron density profile with components using a scattering density profile (SDP) procedure (Kučerka et al., 2008). The SDP procedure guarantees an important relation between the molecular area A and the zeroth order X-ray form factor $F(0)$ (Nagle and Wiener, 1989):

$$AF(0) = 2(n - \rho_W V),$$

where V is the measured volume of the lipid mixture as a function of temperature, $n = n_{DMPC} + n_{CL}f/(1-f)$ is the total, n_{DMPC} is the DMPC and n_{CL} is the TMCL number of electrons, f is the mole fraction of TMCL/(TMCL + DMPC) and ρ_W is the electron density of water as a function of temperature. Informed by our volume measurements, we constrained the volume of the mixture. We also constrained the volume of the headgroup by estimating a headgroup volume for TMCL (506 Å^3) by subtracting the measured ½V_L of TMCL (1040 Å^3) from V_L of DMPC at 50 °C (1118 Å^3) (Nagle and Wilkinson, 1978), where both lipids are in the fluid phase, then subtracting this difference from the headgroup volume of a PC lipid (331 Å^2) (Tristram-Nagle et al., 2002), and multiplying by 2. We also constrained the Gaussian sigma widths of the lipid headgroup peaks to 2–3 Å, the methyl trough Gaussian sigma to 2 Å (corresponding to FWHM of 5 Å) and the width of the hydrocarbon interface to 2.4 Å. The methyl trough had a tendency to get narrower than $\sigma = 2$ Å, which is physically unrealistic for a fluid phase lipid. The difference in distance D_{H1} between the maximum in the electron density profile and the Gibbs dividing surface for the hydrocarbon region was loosely constrained to 4.95 Å. Otherwise, the locations of the components remained free to provide estimates for the head–head distance as previously described (Kučerka et al., 2004). We also fit the X-ray $|F(q_z)|$ data using the mole fractions, 2TMCL/(DMPC + 2TMCL), where TMCL is ½TMCL. The purpose of this was to compare TMCL as a lipid similar to DMPC, with 2 chains of 14 carbons each, with its total volume, headgroup volume and electrons divided in half.

2.3.3. WAXS

The analysis of wide-angle X-ray scattering (WAXS) data has been described previously (Mills et al., 2008a,b). Briefly, the orientational order parameter, S_{Xray}, describes chain order and is similar to an NMR order parameter. S_{Xray} was calculated following the procedure of (Mills et al., 2008a).

2.4. Differential scanning calorimetry (DSC)

DSC measurements were performed using a GE/Microcal VP-DSC (Northhampton, MA) at a heating rate of 60 °C/h and under an extra constant pressure of ~1.5 atm to prevent degassing during the scan. The VP-viewer package was used for data acquisition. 500 μl of a 1 mg/ml MLV sample of TMCL/DMPC mixtures was loaded into the sample cell and 500 μl water was loaded into the reference cell. Samples were cooled to 10 °C and held at this temperature for 10 min before they were scanned. After sample removal, the sample cell was washed by flowing ~500 ml MilliQ water with a vacuum apparatus; evidence of complete removal of the sample was obtained by scanning water vs. water to observe a smooth baseline. Baselines were subtracted using Origin 8 software (OriginLab, Inc., Northampton, MA). Two melting temperatures (solidus and liquidus) were determined by using the Peak Fitting Module. After DSC, TLC revealed considerable damage, ~20–30% lysolecithin. Since the DSC samples were hydrated similarly to the densimetry samples by temperature cycling, this damage did not result from the hydration procedure. The DSC samples were promptly stored in the refrigerator after scanning, so we conclude that these dilute solutions of DMPC/TMCL mixtures may have been degraded during the DSC scan, even though these scans took only 35 min.

2.5. Molecular dynamics simulations

The coarse-grained MD (CGMD) simulations of lipid bilayer systems were carried out with the MARTINI force field (Marrink et al., 2007), which uses a mapping of approximately four heavy atoms to one CG bead. The CG model of 4-myristoyl cardiolipin (TMCL) was obtained by modifying the tails of a previously used 4-oleoyl cardiolipin model (Arnarez et al., 2013) to match those in the MARTINI DMPC model. Two different lipid bilayer systems, pure DMPC and DMPC containing 20% TMCL, were studied. CGMD simulations were performed using the GROMACS v. 4.5.4 MD package (Hess et al., 2008). Initially, the system was minimized, and a 20 ns NVT ensemble equilibration was followed by a 20 ns NPT ensemble equilibration. Each MD run was carried out to cover 500 ns. A 40 fs time step was used to integrate the equations of motion. Electrostatic interactions were shifted smoothly to 0 in the range from 0.0 to 1.2 nm to avoid cut-off artifacts. Similarly, Lennard–Jones interactions were shifted to 0 in the range from 0.9 to 1.2 nm. The pure DMPC system was composed of 320 DMPC lipids and 8317 water beads, and the DMPC–20%TMCL system was composed of 320 DMPC, 80 TMCL, 13022 water molecules and 160 Na^+ ions. Temperature (310 K) and pressure were controlled using the velocity rescale (*V*-rescale) thermostat (Bussi et al., 2007) and Parrinello–Rahman barostat (Parrinello and Rahman, 1981), respectively, with coupling times of 1 and 12 ps. For both bilayer systems semi-isotropic pressure coupling was used, with a compressibility of $3e^{-4}$ bar^{-1}. Simulations were run at 310 K and at 1 atm during NPT runs. For all simulations, visualization and analysis were performed using the VMD v. 1.9 visualization software (Humphrey et al., 1996), using the last frame in the 500 ns trajectory for the snapshots. Number densities were determined using the undulation correction method with filter cutoff $q_0 = 1.0$ nm^{-1} (Brandt et al., 2011; Braun et al., 2011). Areas were calculated by dividing the size of the simulation box (XY) by half the number of lipids.

3. Results

3.1. LAXS and DSC

Fig. 1 shows the LAXS CCD images of fully hydrated, fluctuating samples of pure DMPC (A), TMCL/DMPC mixtures (B, C) and pure TMCL (D). The *D*-spacings shown in Fig. 1 caption were recorded during the sample hydration at CHESS. In (A), the neutral lipid, DMPC, reached its fully hydrated *D*-spacing of 62 Å and did not

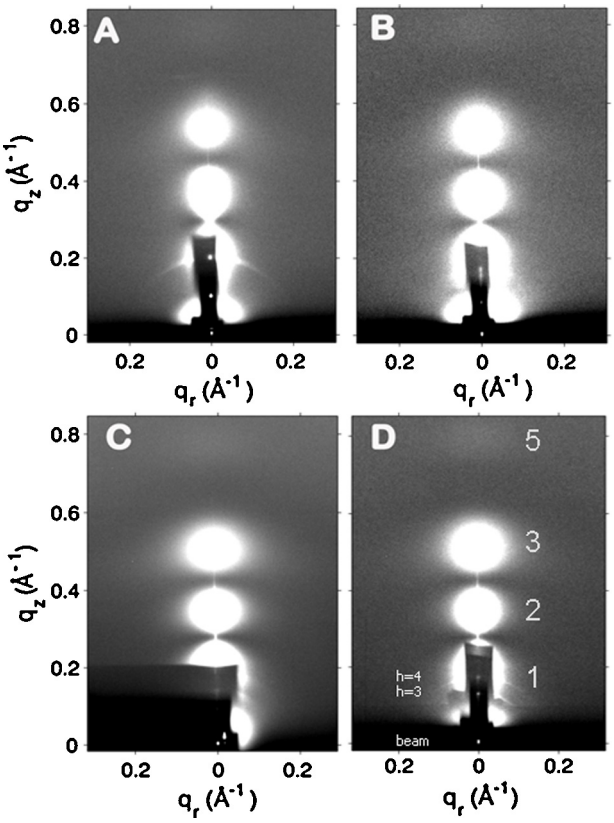

Fig. 1. LAXS of TMCL/DMPC mixtures. (A) DMPC (T = 35 °C), (B) DMPC/4.4 mol% TMCL (T = 35 °C), (C) DMPC/20 mol% TMCL (T = 40 °C) and (D) TMCL (T = 50 °C). Lobes of white, diffuse scattering (large numbers) and lamellar orders (h = 3,4) are visible in (D). The semi-transparent molybdenum beamstop is a thin, vertical "finger" in (A), (B) and (D), and a dark rectangle in (C). In (C), a small spillover from the main beam is visible at q_z and $q_r \approx 0.02$ Å^{-1}. The lamellar D-spacings of these samples are: (A) 62 Å, (B) 77 Å (U), (C) 140 Å (U) and (D) 131 Å (U).

swell further. In (B), (C) and (D), the negative charge of TMCL caused these samples to unbind (U), i.e., to swell continuously. We also observed unbinding in capillary samples with as little as 1.3 mol% TMCL, which was not neutralized by 50 mM Hepes buffer. Previous calorimetry of DMPC with TMCL at <5 mol% in small unilamellar vesicles (Klösgen, unpublished) revealed that all transitions were completed by 35 °C, so our initial experiments of DMPC, 0.7 mol% TMCL, 2.7 mol% TMCL and 4.4 mol% TMCL were carried out at 35 °C. At 20 mol% TMCL, WAXS revealed a gel/fluid phase coexistence at 35 °C, so the temperature was raised to 40 °C in order for this sample to remain in the fluid phase. Similarly for pure TMCL, a gel/fluid phase coexistence prevailed at 45 °C, so the temperature was raised to 50 °C, where the sample was in the fluid phase. Additional calorimetry confirmed these higher phase transition temperatures (see Figs. 2 and 3).

In Fig. 2, the DSC trace of 20 mol% TMCL (blue line) has one melting temperature at ~35 °C, with a broader component extending above 45 °C. This trace, as well as all the mixtures, was decomposed into two melting transitions using software from OriginLab. The lower transition temperature corresponds to the first melting of the combined gel phase (solidus transition) while the upper transition corresponds to final melting of the gel phase from the gel/fluid phase coexistence region (liquidus transition). These transition temperatures are plotted vs. the lipid chain concentration in Fig. 3. We suggest that the lower transition temperature at 20 mol% (33.33 mole TMCL chain %), deviates from linearity due to the fast scan rate of 60 °C/h, and that the upper transition temperature is also elevated for the same reason. In the WAXS data of this sample,

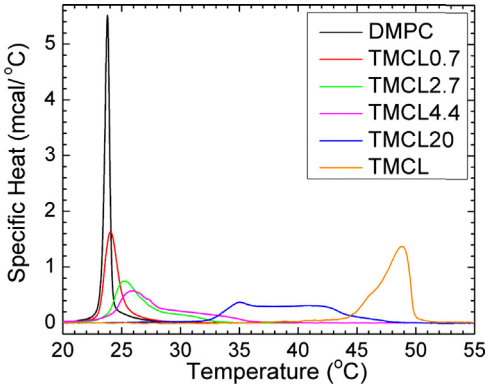

Fig. 2. Differential calorimetry scans of TMCL/DMPC mixtures. Scans of aqueous MLV samples were obtained at 60 °C/h. TMCL0.7 indicates 0.7 mol% TMCL in DMPC + TMCL. (For interpretation of the references to color in the text, the reader is referred to the web version of the article.)

pre-equilibrated and X-rayed at 40 °C, there are no sharp components typical of gel phase *all-trans* chains (Tristram-Nagle et al., 2002). In other words, in contrast to what the DSC results suggest for 20 mol% TMCL (33.33 mole TMCL chain %), at equilibrium in the X-ray experiment, all chain melting is completed by 40 °C.

3.2. Structure

The intensities of the diffuse lobes shown in Fig. 1 are used to obtain the structure of TMCL/DMPC mixtures as described previously (Kučerka et al., 2005a; Lyatskaya et al., 2001; Tristram-Nagle et al., 2010). The first step in the structure determination is to obtain the form factors shown in Fig. 4, which are related to the bilayer electron density profiles through the Fourier transform (Tristram-Nagle and Nagle, 2004). The form factors shown in Fig. 4 have been normalized to the intensity in the second lobe (q_z ~0.25–0.32 Å^{-1}) for ease of comparison. With increasing TMCL concentration, the form factors shift to lower q_z, indicating a membrane thickening. For structure determination, the form factor data are fit to a model of the real-space electron density profile through the Fourier transform using the scattering density profile (SDP) fitting program (Kučerka et al., 2008). An example of an excellent fit of the SDP fitting program to the data is shown in Fig. 5. The fits were equally good using either TMCL or TMCL.

Fig. 6 displays total electron density profiles resulting from the SDP fitting program as a function of increasing TMCL. The presence of TMCL thickens the DMPC host bilayers, which have the same C14:0 chains as guest lipids (TMCL). Pure TMCL has a head-to-head

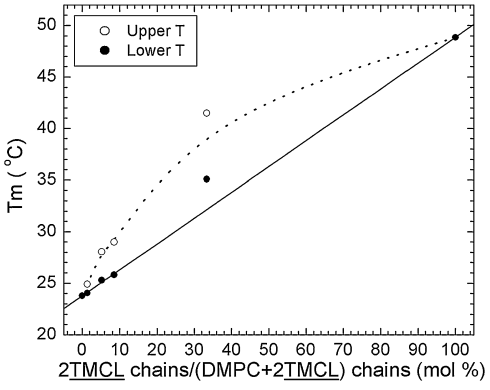

Fig. 3. T_m data (from Fig. 2) vs. concentration of chains in TMCL/DMPC mixtures. Solid straight line shows the solidus melting line and dotted line shows the liquidus melting line.

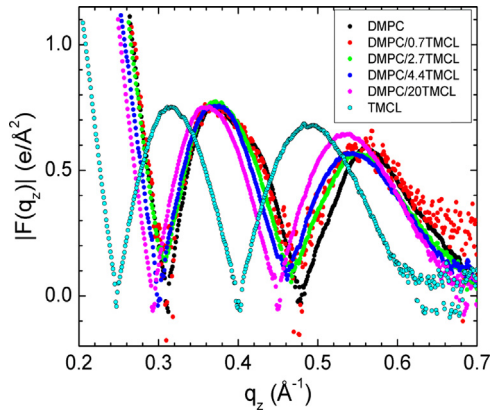

Fig. 4. Form factors for TMCL/DMPC mixtures. The shift in peak positions to lower q_z with increasing TMCL indicates membrane thickening. $T = 35\,^{\circ}C$ (DMPC to DMPC/4.4TMCL), $T = 40\,^{\circ}C$ (DMPC/20TMCL) and $T = 50\,^{\circ}C$ (TMCL).

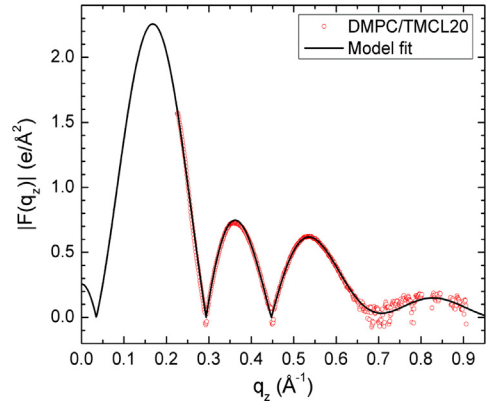

Fig. 5. Model fit to $F(q_z)$ for DMPC/20 mol% TMCL. This is one example of the SDP model fitting program to the diffuse scattering data. $T = 40\,^{\circ}C$.

thickness that is 6 Å greater than that of pure DMPC. Fig. 7 shows the total electron density profile for pure TMCL at 50 °C and the contributions from the diverse components (defined in the figure caption). The methyl trough tended to be more narrow than typical lipids (Kučerka et al., 2005a), and the distance between the GC and the phosphate groups was smaller than many PC lipids we have investigated.

Fig. 8 shows area/lipid for TMCL/DMPC mixtures. As noted previously, in order to maintain the lipid mixture in the fluid phase, the temperature was incrementally increased with increasing amounts

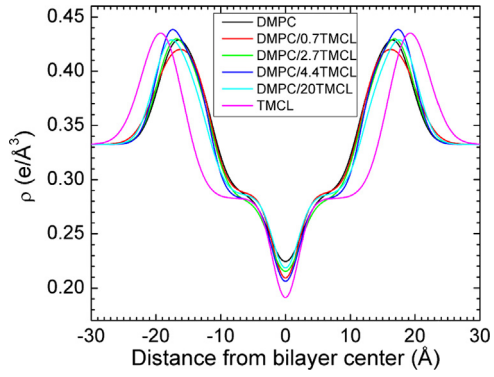

Fig. 6. Electron density profiles of TMCL/DMPC mixtures. TMCL causes the DMPC bilayer to thicken.

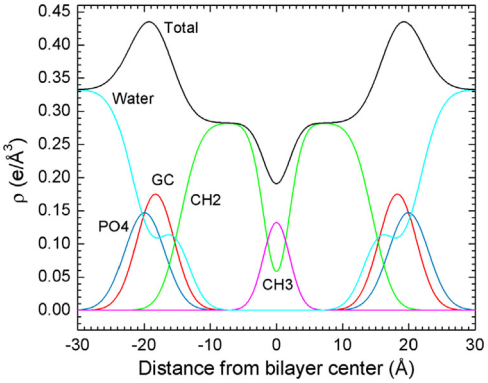

Fig. 7. Electron density profile of pure TMCL at 50 °C in the fluid phase. Component groups are labeled: PO_4, phosphate; GC, glycerol-carbonyl; CH_2, methylene; CH_3, terminal methyl group.

of TMCL. In Figs. 6 and 8, at TMCL/(DMPC + TMCL) < 10 mol%, $T = 35\,^{\circ}C$; at 20 mol%, $T = 40\,^{\circ}C$; and at 100 mol%, $T = 50\,^{\circ}C$. Although it would have been preferable to collect all of the X-ray data at 50 °C, we began these experiments with low TMCL concentrations which were all in the fluid phase at 35 °C. With increasing mol% TMCL, the protocol had to be changed, due to gel/fluid phase coexistence observed in the WAXS data at CHESS. Temperature corrections can be made, estimating that the areal expansivity for TMCL/DMPC mixtures is similar to that of dioleoylphosphatidylcholine (DOPC) (0.0029/deg) (Pan et al., 2008). Increasing the temperature by 15 °C would introduce an error of ~4% in our determined area at 50 °C; correcting back to 35 °C for this error, the pure TMCL area would be smaller, ~104 $Å^2$. The corrected thickness would be larger by 0.6 Å. Since the temperature corrections for these DMPC/TMCL mixtures are not known precisely, error bars in Fig. 8 represent larger corrections (8% in area and 2% in thickness). The fluid phase data were fit using the full TMCL (circles) or using TMCL (½TMCL) (squares), where the amount of TMCL is multiplied by two. As shown, either way of fitting the data gives a similar increase in thickness. However, the average area/lipid decreases for TMCL, since the total volume decreases as more TMCL is added. In pure TMCL, the area is exactly half that obtained for pure TMCL, and it should be multiplied by two to obtain the actual area of TMCL at 50 °C, 108.6 $Å^2$. The purpose of fitting the data with TMCL as well as TMCL is that TMCL is very similar to DMPC, and so it is a check on the use of the SDP data fitting program. The gel phase data are shown as diamonds.

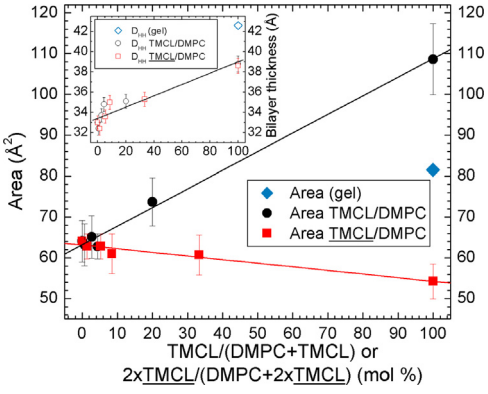

Fig. 8. Area/lipid and bilayer thickness (inset) for TMCL/DMPC and TMCL/DMPC mixtures. Values were determined using volume information and the SDP model fitting program. Fluid phase data are circles (TMCL/DMPC) and squares (TMCL/DMPC), and gel phase data are diamonds. Temperatures are as in Fig. 4.

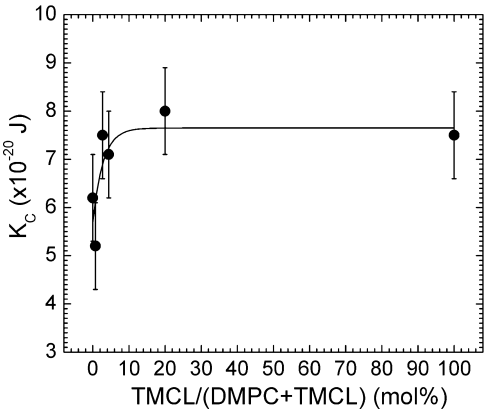

Fig. 9. K_C, bending modulus, for TMCL/DMPC mixtures. Solid line is an exponential fit as a visual guide. Errors result from multiple X-ray exposures at different lateral positions on the same sample and from sample variability.

3.3. Bending modulus, K_C

Fig. 9 shows the results for bending modulus, K_C, obtained by fitting our data to liquid crystal theory (Lyatskaya et al., 2001). Even small amounts of TMCL increase the bending modulus by ~50%, indicating that TMCL stiffens the DMPC membrane. As in previous figures, at TMCL/(DMPC + TMCL) < 10 mol% TMCL, $T = 35\,^{\circ}C$; at 20 mol% TMCL, $T = 40\,^{\circ}C$; and at 100 mol% TMCL, $T = 50\,^{\circ}C$. Since the temperature dependence of K_C is very small for DMPC (Pan et al., 2009) at temperatures outside of the anomalous swelling regime (Chu et al., 2005), we suggest there are negligible temperature corrections to these values.

3.4. TMCL gel phase

After equilibration at 50 °C for ~1 h in the fluid phase, the pure TMCL sample was held at 35 °C for ~2 h, in its gel phase. Although the LAXS looked fairly typical of a gel phase lipid with sharp lamellar orders at first, within a few minutes this sample began to fluctuate and produce diffuse scattering lobes shown in Fig. 10, similar to a fluid phase lipid sample. Over 2 h, the lamellar *D*-spacing increased from 70 Å to >100 Å as the negatively charged layers unbound from each other. This is our first observation of fluctuations in a gel phase lipid.

It was of interest to obtain WAXS of the gel phase TMCL at 35 °C, to investigate if the Bragg rod scattering typical of *all-trans* chains in the gel phase (Tristram-Nagle et al., 1993) occurs in TMCL. WAXS revealed an equatorial chain scattering with no off-equatorial peaks, indicating untilted chains. The equatorial scattering consisted of a single, strong 2,0 peak, $d = 4.2$ Å (see Fig. 11). Using hexagonal packing geometry, the area/chain, A_C, is calculated as $(2 \times 4.2 \times 4.2)/\sqrt{3} = 20.37\,\text{Å}^2$. Since there are 4 chains, $A_{L\text{-gel}} = 4 \times A_C = 81.5\,\text{Å}^2$, which is smaller than the fluid phase area, $A_{L\text{-fluid}} = 108.6\,\text{Å}^2$, *T*-corrected to $104\,\text{Å}^2$ at 35 °C. Since this sample displayed diffuse scattering, we were able to determine its bilayer thickness in a manner similar to fluid phase data. Consistent with this smaller area, the TMCL gel phase D_{HH} at 35 °C is thicker (42.6 Å) than the TMCL fluid phase D_{HH} at 50 °C (38.6 Å, *T*-corrected to 39.2 Å at 35 °C).

3.5. S_{Xray}

X-ray diffuse scattering in the wide-angle region provides an estimate of the chain order, S_{Xray} (Mills et al., 2008a). We use fully hydrated lipid membranes to obtain WAXS data similar to that in Fig. 12 (pure TMCL at 50 °C) from which we calculate S_{Xray}

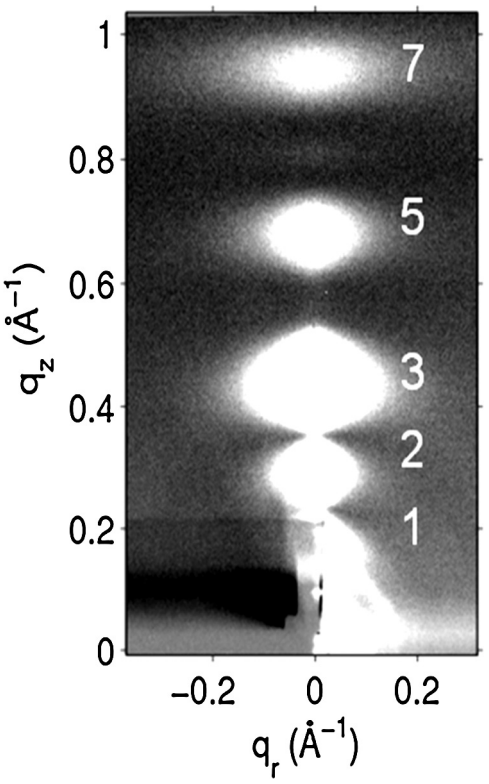

Fig. 10. Diffuse LAXS from gel phase TMCL at 35 °C. Seven lobes of white, diffuse scattering are shown by large numbers. The lamellar *D*-spacing of this sample is 122 Å.

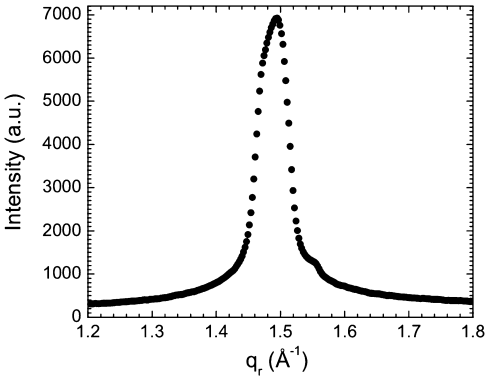

Fig. 11. Intensity plot of WAXS of gel phase TMCL at 35 °C. 2,0 peak intensity was obtained by radially integrating from 2° to 5° relative to the equator.

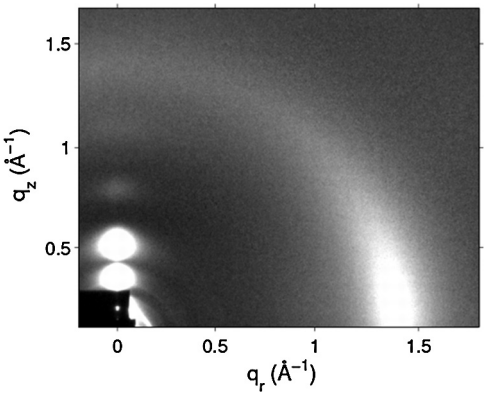

Fig. 12. Fluid phase hydrated WAXS from pure TMCL at 50 °C. The lamellar *D*-spacing of this sample is 95 Å and the interchain *D*-spacing is 4.52 Å.

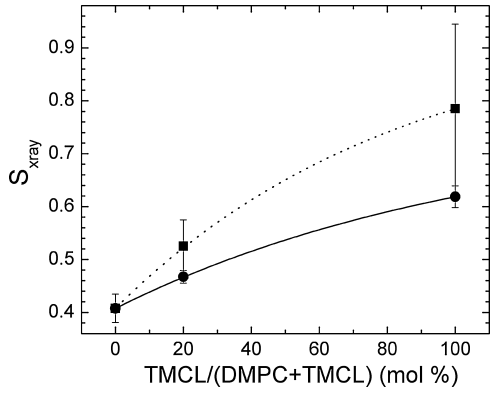

Fig. 13. S_{Xray} for DMPC (35 °C), DMPC/20 mol% TMCL (40 °C) and TMCL (50 °C). Circles are uncorrected, and squares are temperature-corrected values.

for TMCL/DMPC mixtures following (Mills et al., 2008a). Water background was removed from all samples and S_{Xray} results were calculated as described in Section 2.

Fig. 13 reveals that the orientation order parameter, S_{Xray}, increases as TMCL is added to DMPC, i.e., the presence of TMCL induces order in the DMPC chains. As in previous figures, the temperatures of these data points are different, due to the necessity of keeping the sample in the fluid phase. The temperatures are: DMPC (35 °C), 20 mol% TMCL/(DMPC + TMCL) (40 °C) and pure TMCL (50 °C). A temperature correction can be applied to these values, assuming that the temperature correction (0.011/°C) is the same as that of DPPC:DOPC (1:1) mixtures (Mills, 2007). When these values are temperature-corrected back to their value at 35 °C, the S_{Xray} values increase as shown by the squares in Fig. 13. Since the precise S_{Xray} temperature corrections for TMCL/DMPC mixtures are not known, error bars for the temperature-corrected values (squares) represent a larger correction (0.022/°C). Error bars for the original data (circles) result from analyzing several WAXS images for the same sample.

3.6. CGMD simulations

To understand the underlying principles of the X-ray results, simulations were performed on a pure DMPC bilayer and on a bilayer consisting of an 80:20 molar mixture of DMPC and TMCL. Because the time scales required for the proper mixing and relaxation are on the order of hundreds of nanoseconds, 500 ns simulations were performed using a coarse-grained Martini model. The simulations gave area results, corrected for the undulations of a large simulation, for DMPC = 62 Å^2 and DMPC/20 mol% TMCL = 70 Å^2, which can be compared to the experimental results, DMPC = 64 Å^2 and DMPC/20 mol% TMCL = 74 Å^2 (see Fig. 8). In previous work, we found the area of DMPC to be 60.6 Å^2 at 30 °C (Kučerka et al., 2005a), smaller than the current value, even considering the 7° temperature decrease. We are not sure of the basis for this discrepancy, but it could involve a different Lot # of DMPC. Since the present samples were prepared with the same DMPC as their controls, we need to compare our new results with the higher DMPC area of 64 Å^2 measured in this study.

A snapshot from the final frame of the 500 ns DMPC/20 mol% TMCL CGMD simulation is shown in Fig. 14. The CGMD simulation reveals that the headgroups of TMCL (yellow) are positioned near the glycerol-carbonyl groups of DMPC (pink), and deeper into the bilayer than the phosphocholine groups of DMPC (gray-blue).

In order to quantitate the headgroup positions, the number densities obtained from the CGMD simulation were calculated and are shown in Fig. 15B. The position of the TMCL headgroups is near the location of the glycerol-carbonyl groups of DMPC. When the

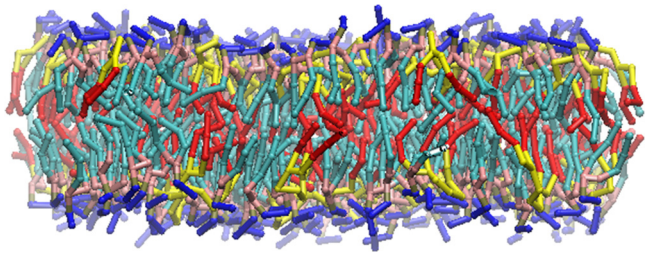

Fig. 14. Snapshot from a CGMD Martini simulation of DMPC/20 mol% TMCL at 310 K. Color coding is TMCL headgroups (yellow), TMCL chains (red), DMPC glycerol-carbonyl groups (pink), DMPC phosphocholine group (gray-blue), and DMPC chains (cyan). (For interpretation of the references to color in this figure legend, the reader is referred to the web version of the article.)

phosphate peak position in DMPC/20 mol% TMCL was compared to that in DMPC (Fig. 15A), a thickening of 2 Å was found, just the same as the 2 Å thickening caused by 20 mol% TMCL in the X-ray electron density profiles (see Fig. 6). In addition, some chain interdigitation may occur in the TMCL chains, since the methyl trough is missing (Fig. 15B).

4. Discussion

In this work we have used X-ray diffuse scattering, DSC and CGMD simulations to probe the structure, thermodynamics and elastic properties of TMCL and mixtures of DMPC and TMCL. Our most important finding is that the presence of TMCL increases the thickness of the host fluid phase DMPC membranes considerably. The D_{HH} of 38.6 Å at 50 °C determined in this work for fluid phase TMCL is close to that (37.8 Å) determined at 55 °C by Lewis et al. (2007) by X-raying MLVs of TMCL in excess water. A thickness increase of ~6 Å from pure DMPC to pure TMCL is similar to that produced by 30 mol% cholesterol in DMPC membranes (Pan et al., 2009), where the increase in D_{HH} was accompanied by a doubling of the S_{Xray} order parameter from 0.4 to 0.8. The order parameter, S_{Xray}, increases due to chain straightening (Mills et al., 2008a), which in turn causes a thickening of the bilayer. In the current work, we observe a doubling of S_{Xray} from 0.4 to 0.8 after correcting for the 15 °C temperature increase needed to maintain TMCL in the fluid phase (Fig. 13). It is known that inner mitochondrial membranes (IMMs) contain little cholesterol (Daum, 1985), which stems from this organelle's bacterial origin. Therefore, in order to increase the membrane thickness to match that of the energy-producing proteins in IMM, another lipid must carry out this function; it appears that CL is well-suited for this job. As mentioned in Section 1, CL co-isolates with many of the proteins involved in oxidative phosphorylation. A recent article that used an upgraded PPM (positioning of protein in membranes) method to calculate hydrophobic thicknesses of many cellular proteins, found an average thickness of nine IMM membrane proteins to be 28.6 ± 1.4 Å (Pogozheva et al., 2013). This thickness is very close to the hydrocarbon thickness of TMCL reported in this study, $2D_C$ = 29 Å. $2D_C$ results from our SDP fitting program and is smaller than D_{HH} shown in Fig. 8. (For nomenclature, refer to Nagle and Tristram-Nagle, 2000.) Evidently, TMCL's hydrophobic thickness is well matched to that of the average IMM protein. The natural form of CL has generally more carbons making it thicker, but also more unsaturation making it thinner (Daum, 1985). Overcoming hydrophobic mismatch between a protein's hydrophobic core and the surrounding membrane is an important concept in membrane biophysics (Botelho et al., 2006; Hwang et al., 2003; Soubias et al., 2008) and could be the primary reason why CL is located in the IMM but less so in the outer mitochondrial membrane (OMM). The average hydrophobic thickness of most of the OMM proteins (β-barrels) is 23 ± 1.0 Å (Pogozheva et al., 2013),

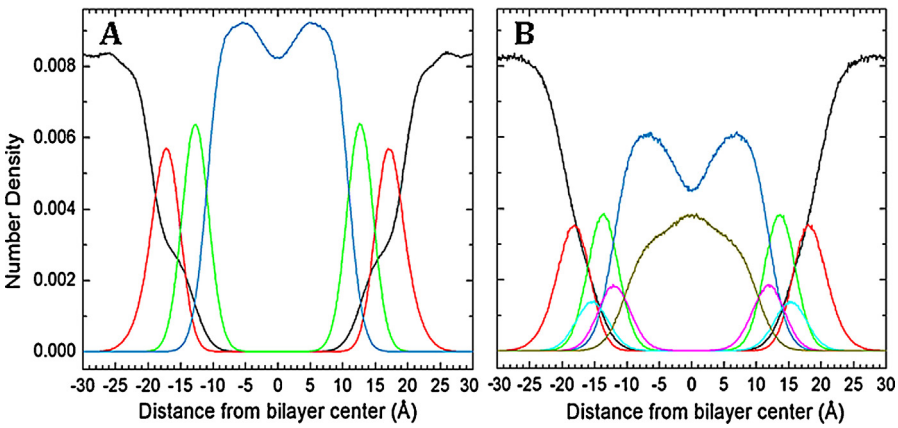

Fig. 15. Number densities calculated from the CGMD Martini simulation of (A) DMPC and (B) DMPC/20 mol% TMCL. Color coding is water (black), DMPC phosphocholine (red), DMPC glycerol-carbonyl (green), TMCL phosphoglycerol (cyan), TMCL glycerol-carbonyl (magenta), DMPC chains (blue) and TMCL chains (dark yellow). (For interpretation of the references to color in this figure legend, the reader is referred to the web version of the article.)

considerably thinner than the IMM proteins. In a related role, using an EPR spin probe to measure membrane order, Yamauchi et al. (1981) showed that CL native to *Tetrahymena pyriformis* acts to maintain membrane fluidity, similar to cholesterol's role in fluidizing the gel phase and rigidifying the fluid phase.

Besides thickening membranes, CL acts similarly to cholesterol in another way. We have previously investigated water permeability through membranes and found that cholesterol decreased water permeability in a concentration dependent manner, as the area/lipid decreased (Mathai et al., 2008). Similarly, Shibata et al. (1994) found that bovine heart CL halved water permeability even at low concentrations (~3 mol%). In the IMM, with negligible amounts of cholesterol, CL may take on the important role of reducing water leakage. Since the area/lipid condenses when TMCL is added to DMPC (see Fig. 8), this could be the cause of the decrease in permeability.

Haines and Dencher (2002) suggested that one other, or additional, potential reason for CL's close association with energy-producing proteins is to serve as a storage site for protons that are generated during ATP production. With a second phosphate pK_a above 8, CL has a high buffering capacity (Haines and Dencher, 2002). The structure of the acid-anion that would serve as a proton storage site could require the CL headgroup to be sequestered away from the positively charged choline groups of PC lipids so that its acid-anion would not be neutralized. As shown in Fig. 7, the distance between the PO_4-group and the CG-group in fluid phase TMCL is ~2 Å. This distance is smaller than we have found in PC lipids (3.5–4 Å) (Kučerka et al., 2005a,b), indicating that the two phosphate groups must be nearly parallel to the membrane surface, and at nearly the same level as the CG groups. In an NMR study, Pinheiro et al. (1994) calculated that the P-N vector of PC lipids tilts downward toward the membrane surface in the presence of the negatively charged CL. In our TMCL/DMPC X-ray electron density profiles, we cannot distinguish the DMPC choline group from its phosphate group, since their electron densities are combined. In the snapshot from the coarse-grain MD simulation shown in Fig. 14, and the number density positions shown in Fig. 15, the TMCL headgroups in the DMPC/20 mole% mixture are sequestered underneath the DMPC phosphate groups, closer to the DMPC glycerol-carbonyl groups. This is yet another way of pointing out that TMCL is similar to cholesterol, in that its headgroup is covered by the phosphocholine umbrella (Brown and Seelig, 1978; Huang and Feigenson, 1999).

Other investigations have referred to the "small headgroup" of CL (Haines, 2009; Lewis and McElhaney, 2009; Nichols-Smith and Kuhl, 2005). Our volume results are summarized in Table 1. When compared to the PC headgroup volume (331 Å^3) (Tristram-Nagle et al., 2002), the ½TMCL headgroup is ~76% of that volume, so it is smaller, but not exceedingly small. We can compare ½TMCL headgroup determined herein (253 Å^3) to that of the PG headgroup (291 Å^3) (Pan et al., 2012) and note that it is smaller by only 13% (see Table 1). We did explore the effect of salt using 50 mM Hepes buffer, pH 7.0, but found little effect on bilayer structure at low mol% TMCL, so we did not pursue this at higher mol%. Our DSC and X-ray results determined that the T_m of TMCL is 49 °C in pure water, which is higher than two values reported in (Lewis et al., 2007). In that work, TMCL melted at 38.9 °C in 100 mM Tris buffer and at 41.2 °C in 50 mM phosphate buffer, both containing 150 mM NaCl. Evidently these higher salt concentrations stabilize the fluid phase and it is known that divalent cations induce the H_{II} phase (Rand and Sengupta, 1972). It is difficult to add salt to our oriented samples in controlled concentrations, particularly when the samples unbind, i.e., swell during hydration. Therefore we chose to focus on samples hydrated from pure water.

Table 1
Volume results.

Lipid	Lipid volume (Å^3) at 50 °C	4-Chain headgroup volume (Å^3)	2-Chain headgroup volume (Å^3)
TMCL	2080	506	253
DMPC	1118	–	331
DMPG[a]	1075	–	291 ± 4

[a] Pan et al. (2012).

Since CL is primarily associated with proteins, several groups have investigated the ability of CL to phase separate when mixed with other lipids. (Frias et al., 2011) mixed CL with dimyristoylphosphatidylethanolamine (DMPE) and used DSC and FTIR to determine that CL and DMPE are poorly miscible across a broad composition range. Poor immiscibility of unsaturated CL with dipalmitoylphosphocholine (DPPC) and dipalmitoylphosphoethanolamine (DPPE) has also been observed (Sennato et al., 2005), but this was a case of gel/fluid domain formation. We also tested our TMCL/DMPC mixtures for domain formation. In the analysis of S_{Xray}, it is possible to analyze the WAXS data of the 20 mol% TMCL/(DMPC + TMCL) mixture using a two-decay fit instead of a single-decay fit (Mills et al., 2008b). The presence of two liquid domains is indicated when a two-decay fit has a smaller root mean square deviation than the single-decay fit. Our analysis showed no improvement of a two-decay fit over a single-decay fit, so we suggest that there is no domain formation in the 20 mol% TMCL/(DMPC + TMCL) mixture. The course of our DSC solidus T_m line did exhibit ideal mixing at

low mole percentages (Fig. 3). This supports the finding that there is no domain formation. In addition, in the MD simulation, there was no visible aggregation of TMCL (Fig. 14). Therefore, we conclude that the TM form of CL, when mixed with DMPC, does not form domains.

Another interesting result from our study is the observation that TMCL increases the bending modulus, K_C, or stiffness of the host DMPC membrane, even at low inoculation. The 50% increase is significant, even though it is small compared to the effect of 30 mol% cholesterol in DMPC (increase in K_C = 550%) (Pan et al., 2009). Still, the presence of TMCL modifies the membrane bending modulus in the direction of membrane stiffening, not membrane softening. In apparent contrast, (Lewis et al., 2007) found that the η value, which is proportional to the inverse of K_C, increases by a factor of 3 compared to PC dispersions, indicating a softening of pure TMCL membranes. The 50% increase in K_C that we observe is compatible with the increase in membrane thickness and the increase in membrane order, S_{Xray}, for this species of CL (TMCL). Since the methods in Lewis et al. (2007) do not directly determine K_C, rather the product of K_C times B, the bulk modulus, our two results may not be in disagreement that the bilayer is stiffened by TMCL.

While TMCL stiffens, orders and thickens the DMPC fluid phase membrane, it may seem like a contradiction that area/lipid also increases. Usually A_L and D_{HH} are inversely related; e.g., when a gel phase lipid melts into its fluid phase, A_L increases while the bilayer thins. This apparent contradiction arises when TMCL is treated as a 2-chain lipid, even though this 4-chain lipid is roughly twice the size of DMPC. Upon addition of the much larger TMCL to DMPC, the apparent A_L of DMPC increases. Another way to think about these experiments is to cut the TMCL in half, TMCL, and double its concentration. In this case (see Fig. 8), the apparent A_L decreases. Although we also performed this analysis, we prefer the analysis that shows an increase in A_L, in order to compare to the MD simulations, which also show an increase in the average A_L at 20 mol% TMCL. Another surprising result is that TMCL, with the same chains as DMPC, orders and stiffens the membrane, leading to an increase in thickness. Why does this happen, even when some chain interdigitation of TMCL may occur, as suggested by Prossnigg et al., 2010, for a TMCL/gel phase lipid mixture? It can only be due to the headgroup configuration of TMCL creating a more rigid molecule than DMPC. The acid-anion that is a resonance structure (Haines, 2009) must confer a stability on the upper part of the TMCL lipid that orders chains and thus thickens the bilayers. Future NMR experiments could shed light on this question.

Finally we compare our TMCL gel phase results to those published in Lewis et al. (2007). In that work, their gel phase D_{HH} is 43.5 Å and our result is 42.6 Å, in good agreement. Our gel phase area is 81.5 Å^2 while their result is 83.2 Å^2. While the gel phase is not physiologically relevant for mitochondria, it is gratifying to know that two independent X-ray studies determine similar quantities using different sample preparations. As noted in the Results section, TMCL's unusual fluctuations in the gel phase (Fig. 10) enabled us to use the same methods as in the fluid phase to determine its structure. These fluctuations most likely result from the large D-spacing caused by unbinding of layers in the stack due to negative charge repulsion. The TMCL gel phase area of 40.8 Å^2 is smaller than that of gel phase DMPC (47.2 Å^2) at 10 °C (Tristram-Nagle et al., 2002), and roughly equal to that of DLPE (41 Å^2) at 20 °C (Nagle and Tristram-Nagle, 2000), confirming our observation of untilted chains in gel phase TMCL.

Acknowledgments

Research reported in this publication was supported by the National Institute of General Medical Sciences of the National Institutes of Health under award number R01GM44976 (AIB, BWT, and STN), NSF 1144281 (DM and JK-S), and NRSA pre-doctoral fellowship award number F31 NS077634-02 (ARB). The content is solely the responsibility of the authors and does not necessarily represent the official views of the National Institutes of Health. A.I.B. was partially supported by the Howard Hughes Medical Institute (HHMI) for undergraduate research and by the Lipella Company, Pittsburgh, PA. We acknowledge the Cornell High Energy Synchrotron Source (CHESS), which is supported by the National Science Foundation (NSF) and the NIH/NIGMS under NSF award DMR-093684, and we especially thank Dr. Arthur Woll for facilitating our use of the G1 station. The authors would like to thank Thalia Mills for her help with the oriented sample preparation, Dave Bauer for his help with the VP-DSC data collection in the Evilevitch Lab, and Leah Langer for help in determining the number densities. The authors would like to thank Prof. John Nagle for helpful discussions.

References

Arnarez, C., Mazat, J.P., Elezgaray, J., Marrink, S.J., Periole, X., 2013. Evidence for cardiolipin binding sites on the membrane-exposed surface of the cytochrome bc1. J. Am. Chem. Soc. 135, 3112–3120.

Barth, P.G., Scholte, H.R., Berden, J.A., Vanderkleivanmoorsel, J.M., Luythouwen, I.E.M., Vantveerkorthof, E.T., Vanderharten, J.J., Sobotkaplojhar, M.A., 1983. An X-linked mitochondrial disease affecting cardiac muscle, skeletal muscle and neutrophil leukocytes. J. Neurol. Sci. 62, 327–355.

Botelho, A.V., Huber, T., Sakmar, T.P., Brown, M.F., 2006. Curvature and hydrophobic forces drive oligomerization and modulate activity of rhodopsin in membranes. Biophys. J. 91, 4464–4477.

Brandt, E.G., Braun, A.R., Sachs, J.N., Nagle, J.F., Edholm, O., 2011. Interpretation of fluctuation spectra in lipid bilayer simulations. Biophys. J. 100, 2104–2111.

Braun, A.R., Brandt, E.G., Edholm, O., Nagle, J.F., Sachs, J.N., 2011. Determination of electron density profiles and area from simulations of undulating membranes. Biophys. J. 100, 2112–2120.

Brown, M.F., Seelig, J., 1978. Influence of cholesterol on polar region of phosphatidylcholine and phosphatidylethanolamine bilayers. Biochemistry 17, 381–384.

Bussi, G., Donadio, D., Parrinello, M., 2007. Canonical sampling through velocity rescaling. J. Chem. Phys. 126.

Chu, N., Kučerka, N., Liu, Y.F., Tristram-Nagle, S., Nagle, J.F., 2005. Anomalous swelling of lipid bilayer stacks is caused by softening of the bending modulus. Phys. Rev. E 71.

Claypool, S.M., Oktay, Y., Boontheung, P., Loo, J.A., Koehler, C.M., 2008. Cardiolipin defines the interactome of the major ADP/ATP carrier protein of the mitochondrial inner membrane. J. Cell Biol. 182, 937–950.

Dahlberg, M., 2007. Polymorphic phase behavior of cardiolipin derivatives studied by coarse-grained molecular dynamics. J. Phys. Chem. B 111, 7194–7200.

Dahlberg, M., Maliniak, A., 2008. Molecular dynamics simulations of cardiolipin bilayers. J. Phys. Chem. B 112, 11655–11663.

Dahlberg, M., Marini, A., Mennucci, B., Maliniak, A., 2010. Quantum chemical modeling of the cardiolipin headgroup. J. Phys. Chem. A 114, 4375–4387.

Daum, G., 1985. Lipids of mitochondria. Biochim. Biophys. Acta 822, 1–42.

Deng, Y.R., Mieczkowski, M., 1998. Three-dimensional periodic cubic membrane structure in the mitochondria of amoebae (*Chaos carolinensis*) mitochondria determined by electron microscopic tomography. Protoplasma 203, 16–25.

Domenech, O., Morros, A., Cabanas, M.E., Montero, M.T., Hernandez-Borrell, J., 2007. Thermal response of domains in cardiolipin content bilayers. Ultramicroscopy 107, 943–947.

Eble, K.S., Coleman, W.B., Hantgan, R.R., Cunningham, C.C., 1990. Tightly associated cardiolipin in the bovine heart mitochondrial ATP synthase as analyzed by P-31 NMR spectroscopy. J. Biol. Chem. 265, 19434–19440.

Frias, M., Benesch, M.G.K., Lewis, R.N.A.H., McElhaney, R.N., 2011. On the miscibility of cardiolipin with 1,2-diacyl phosphoglycerides: binary mixtures of dimyristoylphosphatidylethanolamine and tetramyristoylcardiolipin. Biochim. Biophys. Acta 1808, 774–783.

Gomez, B., Robinson, N.C., 1999. Quantitative determination of cardiolipin in mitochondrial electron transferring complexes by silicic acid high-performance liquid chromatography. Anal. Biochem. 267, 212–216.

Haines, T.H., 2009. A new look at Cardiolipin. Biochim. Biophys. Acta 1788, 1997–2002.

Haines, T.H., Dencher, N.A., 2002. Cardiolipin: a proton trap for oxidative phosphorylation. FEBS Lett. 528, 35–39.

Hess, B., Kutzner, C., van der Spoel, D., Lindahl, E., 2008. GROMACS 4: algorithms for highly efficient, load-balanced, and scalable molecular simulation. J. Chem. Theory Comput. 4, 435–447.

Hoch, F.L., 1992. Cardiolipins and biomembrane function. Biochim. Biophys. Acta 1113, 71–133.

Hoffmann, B., Stockl, A., Schlame, M., Beyer, K., Klingenberg, M., 1994. The reconstituted ADP/ATP carrier activity has an absolute requirement for cardiolipin as shown in cysteine mutants. J. Biol. Chem. 269, 1940–1944.

Horvath, L.I., Drees, M., Beyer, K., Klingenberg, M., Marsh, D., 1990. Lipid–protein interactions in ADP/ATP carrier egg phosphatidylcholine recombinants studied by spin-label ESR spectroscopy. Biochemistry 29, 10664–10669.
Hostetler, K.Y., Van den Bosch, H., 1972. Subcellular and submitochondrial localization of biosynthesis of cardiolipin and related phospholipids in rat liver. Biochim. Biophys. Acta 260, 380–386.
Hovius, R., Lambrechts, H., Nicolay, K., Dekruijff, B., 1990. Improved methods to isolate and subfractionate rat liver mitochondria: lipid composition of the inner and outer membrane. Biochim. Biophys. Acta 1021, 217–226.
Huang, J.Y., Feigenson, G.W., 1999. A microscopic interaction model of maximum solubility of cholesterol in lipid bilayers. Biophys. J. 76, 2142–2157.
Humphrey, W., Dalke, A., Schulten, K., 1996. VMD: visual molecular dynamics. J. Mol. Graph. Model. 14, 33–38.
Hwang, T.C., Koeppe, R.E., Andersen, O.S., 2003. Genistein can modulate channel function by a phosphorylation-independent mechanism: importance of hydrophobic mismatch and bilayer mechanics. Biochemistry 42, 13646–13658.
Jalmar, O., Francois-Moutal, L., Garcia-Saez, A.J., Perry, M., Granjon, T., Gonzalvez, F., Gottlieb, E., Ayala-Sanmartin, J., Klosgen, B., Schwille, P., Petit, P.X., 2013. Caspase-8 binding to cardiolipin in giant unilamellar vesicles provides a functional docking platform for bid. PLoS ONE 8, e55250.
Jelsema, C.L., Morre, D.J., 1978. Distribution of phospholipid biosynthetic-enzymes among cell components of rat liver. J. Biol. Chem. 253, 7960–7971.
Kagan, V.E., Wipf, P., Stoyanovsky, D., Greenberger, J.S., Borisenko, G., Belikova, N.A., Yanamala, N., Samhan Arias, A.K., Tungekar, M.A., Jiang, J., Tyurina, Y.Y., Ji, J., Klein-Seetharaman, J., Pitt, B.R., Shvedova, A.A., Bayir, H., 2009. Mitochondrial targeting of electron scavenging antioxidants: regulation of selective oxidation vs random chain reactions. Adv. Drug Deliv. Rev. 61, 1375–1385.
Kaplan, R.S., Pratt, R.D., Pedersen, P.L., 1986. Purification and characterization of the reconstitutively active phosphate transporter from rat-liver mitochondria. J. Biol. Chem. 261, 2767–2773.
Kates, M., Syz, J.Y., Gosser, D., Haines, T.H., 1993. pH-dissociation characteristics of cardiolipin and its 2′-deoxy analogue. Lipids 28, 877–882.
Kučerka, N., Kiselev, M.A., Balgavy, P., 2004. Determination of bilayer thickness and lipid surface area in unilamellar dimyristoylphosphatidylcholine vesicles from small-angle neutron scattering curves: a comparison of evaluation methods. Eur. Biophys. J. 33, 328–334.
Kučerka, N., Liu, Y.F., Chu, N.J., Petrache, H.I., Tristram-Nagle, S., Nagle, J.F., 2005a. Structure of fully hydrated fluid phase DMPC and DLPC lipid bilayers using X-ray scattering from oriented multilamellar arrays and from unilamellar vesicles. Biophys. J. 88, 2626–2637.
Kučerka, N., Nagle, J.F., Sachs, J.N., Feller, S.E., Pencer, J., Jackson, A., Katsaras, J., 2008. Lipid bilayer structure determined by the simultaneous analysis of neutron and X-ray scattering data. Biophys. J. 95, 2356–2367.
Kučerka, N., Tristram-Nagle, S., Nagle, J.F., 2005b. Structure of fully hydrated fluid phase lipid bilayers with monounsaturated chains. J. Membr. Biol. 208, 193–202.
Lewis, R.N.A.H., McElhaney, R.N., 2009. The physicochemical properties of cardiolipin bilayers and cardiolipin-containing lipid membranes. Biochim. Biophys. Acta 1788, 2069–2079.
Lewis, R.N.A.H., Zweytick, D., Pabst, G., Lohner, K., McElhaney, R.N., 2007. Calorimetric, X-ray diffraction, and spectroscopic studies of the thermotropic phase behavior and organization of tetramyristoyl cardiolipin membranes. Biophys. J. 92, 3166–3177.
Liu, Y.F., Nagle, J.F., 2004. Diffuse scattering provides material parameters and electron density profiles of biomembranes. Phys. Rev. E 69, 040901–040904.
Lupi, S., Perla, A., Maselli, P., Bordi, F., Sennato, S., 2008. Infrared spectra of phosphatidylethanolamine-cardiolipin binary system. Colloids Surf. B 64, 56–64.
Lyatskaya, Y., Liu, Y.F., Tristram-Nagle, S., Katsaras, J., Nagle, J.F., 2001. Method for obtaining structure and interactions from oriented lipid bilayers. Phys. Rev. E 63, 0119071–0119079.
Mathai, J.C., Tristram-Nagle, S., Nagle, J.F., Zeidel, M.L., 2008. Structural determinants of water permeability through the lipid membrane. J. Gen. Physiol. 131, 69–76.
Mills, T.T., 2007. Wide angle X-ray scattering probes chain order and identifies liquid–liquid phase coexistence in oriented lipid membranes. In: Field of Biophysics. Cornell University, Ithaca, NY, pp. 273.
Mills, T.T., Toombes, G.E.S., Tristram-Nagle, S., Smilgies, D.M., Feigenson, G.W., Nagle, J.F., 2008a. Order parameters and areas in fluid-phase oriented lipid membranes using wide angle X-ray scattering. Biophys. J. 95, 669–681.
Mills, T.T., Tristram-Nagle, S., Heberle, F.A., Morales, N.F., Zhao, J., Wu, J., Toombes, G.E.S., Nagle, J.F., Feigenson, G.W., 2008b. Liquid–liquid domains in bilayers detected by wide angle X-ray scattering. Biophys. J. 95, 682–690.
Nagle, J.F., Tristram-Nagle, S., 2000. Structure of lipid bilayers. Biochim. Biophys. Acta – Rev. Biomembr. 1469, 159–195.
Nagle, J.F., Wiener, M.C., 1989. Relations for lipid bilayers – connection of electron-density profiles to other structural quantities. Biophys. J. 55, 309–313.
Nagle, J.F., Wilkinson, D.A., 1978. Lecithin bilayers – density measurements and molecular interactions. Biophys. J. 23, 159–175.
Nichols-Smith, S., Kuhl, T., 2005. Electrostatic interactions between model mitochondrial membranes. Colloids Surf. B 41, 121–127.
Nichols-Smith, S., Teh, S.Y., Kuhl, T.L., 2004. Thermodynamic and mechanical properties of model mitochondrial membranes. Biochim. Biophys. Acta 1663, 82–88.
Pan, J., Tristram-Nagle, S., Kucerka, N., Nagle, J.F., 2008. Temperature dependence of structure, bending rigidity, and bilayer interactions of dioleoylphosphatidylcholine bilayers. Biophys. J. 94, 117–124.
Pan, J., Heberle, F.A., Tristram-Nagle, S., Szymanski, M., Koepfinger, M., Katsaras, J., Kucerka, N., 2012. Molecular structures of fluid phase phosphatidylglycerol bilayers as determined by small angle neutron and X-ray scattering. Biochim. Biophys. Acta 1818, 2135–2148.
Pan, J., Tristram-Nagle, S., Nagle, J.F., 2009. Effect of cholesterol on structural and mechanical properties of membranes depends on lipid chain saturation. Phys. Rev. E 80, 021931.
Parrinello, M., Rahman, A., 1981. Polymorphic transitions in single-crystals – a new molecular-dynamics method. J. Appl. Phys. 52, 7182–7190.
Pfeiffer, K., Gohil, V., Stuart, R.A., Hunte, C., Brandt, U., Greenberg, M.L., Schagger, H., 2003. Cardiolipin stabilizes respiratory chain supercomplexes. J. Biol. Chem. 278, 52873–52880.
Pinheiro, T.J.T., Duralski, A.A., Watts, A., 1994. Phospholipid headgroup–headgroup electrostatic interactions in mixed bilayers of cardiolipin with phosphatidylcholines studied by H-2 NMR. Biochemistry 33, 4896–4902.
Pogozheva, I.D., Tristram-Nagle, S., Mosberg, H.I., Lomize, A.L., 2013. Structural adaptations of proteins to different biological membranes. Biochim. Biophys. Acta 1828, 2592–2608.
Powell, G.L., Hui, S.W., 1996. Tetraoleoylpyrophosphatidic acid: a four acyl-chain lipid which forms a hexagonal II phase with high curvature. Biophys. J. 70, 1402–1406.
Powell, G.L., Marsh, D., 1985. Polymorphic phase-behavior of cardiolipin derivatives studied by P-31 NMR and X-ray diffraction. Biochemistry 24, 2902–2908.
Prossnigg, F., Hickel, A., Pabst, G., Lohner, K., 2010. Packing behaviour of two predominant anionic phospholipids of bacterial cytoplasmic membranes. Biophys. Chem. 150, 129–135.
Raghunathan, M., Zubovski, Y., Venable, R.M., Pastor, R.W., Nagle, J.F., Tristram-Nagle, S., 2012. Structure and elasticity of lipid membranes with genistein and daidzein bioflavinoids using X-ray scattering and MD simulations. J. Phys. Chem. B 116, 3918–3927.
Rand, R.P., Sengupta, S., 1972. Cardiolipin forms hexagonal structures with divalent cations. Biochim. Biophys. Acta 225, 484–492.
Robinson, N.C., 1993. Functional binding of cardiolipin to cytochrome-C-oxidase. J. Bioenerg. Biomembr. 25, 153–163.
Schlame, M., Ren, M.D., Xu, Y., Greenberg, M.L., Haller, I., 2005. Molecular symmetry in mitochondrial cardiolipins. Chem. Phys. Lipids 138, 38–49.
Seddon, J.M., Kaye, R.D., Marsh, D., 1983. Induction of the lamellar-inverted hexagonal phase-transition in cardiolipin by protons and mono-valent cations. Biochim. Biophys. Acta 734, 347–352.
Sennato, S., Bordi, F., Cametti, C., Coluzza, C., Desideri, A., Rufini, S., 2005. Evidence of domain formation in cardiolipin–glycerophospholipid mixed monolayers. A thermodynamic and AFM study. J. Phys. Chem. B 109, 15950–15957.
Shibata, A., Ikawa, K., Shimooka, T., Terada, H., 1994. Significant stabilization of the phosphatidylcholine bilayer structure by incorporation of small amounts of cardiolipin. Biochim. Biophys. Acta 1192, 71–78.
Soubias, O., Niu, S.L., Mitchell, D.C., Gawrisch, K., 2008. Lipid–rhodopsin hydrophobic mismatch alters rhodopsin helical content. J. Am. Chem. Soc. 130, 12465–12471.
Tarahovsky, Y.S., Arsenault, A.L., MacDonald, R.C., McIntosh, T.J., Epand, R.M., 2000. Electrostatic control of phospholipid polymorphism. Biophys. J. 79, 3193–3200.
Tristram-Nagle, S., 2007. Preparation of oriented, fully hydrated lipid samples for structure determination using X-ray scattering. In: Methods in Molecular Biology: Methods in Membrane Lipids. Humana Press, Inc., Totowa, NJ, pp. 63–75.
Tristram-Nagle, S., Kim, D.J., Akhunzada, N., Kucerka, N., Mathai, J.C., Katsaras, J., Zeidel, M., Nagle, J.F., 2010. Structure and water permeability of fully hydrated diphytanoylPC. Chem. Phys. Lipids 163, 630–637.
Tristram-Nagle, S., Liu, Y.F., Legleiter, J., Nagle, J.F., 2002. Structure of gel phase DMPC determined by X-ray diffraction. Biophys. J. 83, 3324–3335.
Tristram-Nagle, S., Nagle, J.F., 2004. Lipid bilayers: thermodynamics, structure, fluctuations, and interactions. Chem. Phys. Lipids 127, 3–14.
Tristram-Nagle, S., Zhang, R., Suter, R.M., Worthington, C.R., Sun, W.J., Nagle, J.F., 1993. Measurement of chain tilt angle in fully hydrated bilayers of gel phase lecithins. Biophys. J. 64, 1097–1109.
Yamauchi, T., Ohki, K., Maruyama, H., Nozawa, Y., 1981. Thermal adaptation of tetrahymena membranes with special reference to mitochondria – role of cardiolipin fluidity of mitochondrial-membranes. Biochim. Biophys. Acta 649, 385–392.
Yu, L., Yu, C.A., King, T.E., 1978. The indispensability of phospholipid and ubiquinone in mitochondrial electron transfer from succinate to cytochrome c. J. Biol. Chem. 253, 2657–2663.
Zhang, M., Mileykovskaya, E., Dowhan, W., 2002. Gluing the respiratory chain together – cardiolipin is required for supercomplex formation in the inner mitochondrial membrane. J. Biol. Chem. 277, 43553–43556.